Gating currents associated with intramembrane charge displacement in HERG potassium channels

David R. Piper*, Anthony Varghese†, Michael C. Sanguinetti*‡§, and Martin Tristani-Firouzi¶

Departments of *Physiology and ¶Pediatrics and ‡Eccles Program in Human Molecular Biology and Genetics, University of Utah, Salt Lake City, UT 84112; and †Department of Medicine, University of Minnesota, Minneapolis, MN 55455

Edited by Ramon Latorre, Center for Scientific Studies, Valdivia, Chile, and approved July 9, 2003 (received for review May 6, 2003)

HERG **(human ether-a-go-go-related gene) encodes a delayed rectifier K^+ channel vital to normal repolarization of cardiac action potentials. Attenuation of repolarizing K^+ current caused by mutations in HERG or channel block by common medications prolongs ventricular action potentials and increases the risk of arrhythmia and sudden death. The critical role of HERG in maintenance of normal cardiac electrical activity derives from its unusual gating properties. Opposite to other voltage-gated K^+ channels, the rate of HERG channel inactivation is faster than activation and appears to be intrinsically voltage dependent. To investigate voltage sensor movement associated with slow activation and fast inactivation, we characterized HERG gating currents. When the cut-open oocyte voltage clamp technique was used, membrane depolarization elicited gating current with fast and slow components that differed 100-fold in their kinetics. Unlike previously studied voltage-gated K^+ channels, the bulk of charge movement in HERG was protracted, consistent with the slow rate of ionic current activation. Despite similar kinetic features, fast inactivation was not derived from the fast gating component. Analysis of an inactivation-deficient mutant HERG channel and a Markov kinetic model suggest that HERG inactivation is coupled to activation.**

voltage clamp | *Xenopus* | ion channel | EAG

HERG (human ether-a-go-go-related gene) is one of many voltage-gated K^+ channels expressed in the heart and brain that act in concert to mediate repolarization of action potentials. Naturally occurring mutations in HERG or channel block by common medications cause long QT syndrome, a disorder of myocellular repolarization that predisposes affected individuals to life-threatening arrhythmias (1). HERG gating is unusual because of its mechanism of inward rectification that reduces outward current at depolarized membrane potentials. Unlike typical inward rectifier K^+ channels, where outward current is blocked by intracellular polyamines and Mg^{2+} (2), rectification of HERG is caused by a combination of voltage-dependent gating processes: rapid inactivation and slow activation (3, 4). Like C-type inactivation in Shaker channels, mutations in the outer mouth of the pore influence inactivation in HERG channels. However, unlike Shaker, inactivation of HERG is $\approx$100 times faster than activation, and appears to be intrinsically voltage dependent and not coupled to activation. For example, a pore mutation (S631A) in HERG selectively shifts the voltage dependence of inactivation by +100 mV without influencing activation (5, 6), and a double mutation (G628C/S631C) eliminates inactivation (3). These findings suggest that the voltage dependency of HERG channel inactivation and activation may be derived from distinct voltage-sensing mechanisms.

Protein rearrangements associated with HERG gating have been monitored by using a fluorescent probe covalently attached to the outer segment of the S4 domain (7). Two voltage-dependent components of fluorescence were described with fast and slow kinetics. The slow component correlated with channel activation and the fast transient in some ways correlated with inactivation. However, gating currents from HERG channels have not been reported and it is unknown whether fast inactivation and slow activation of ionic current are correlated with gating currents with corresponding kinetic components. To investigate the fundamental properties of activation and inactivation pathways, we used the cut-open oocyte vaseline gap voltage clamp technique (8, 9) to record gating currents, presumed to result from intramembrane charge movement associated with translocation of the voltage sensor (10) from WT and mutant HERG channels heterologously expressed in *Xenopus* oocytes.

Materials and Methods

Molecular Biology. Site-directed mutagenesis, *in vitro* synthesis, and injection of cRNA into *Xenopus laevis* oocytes were performed as described (11). Oocytes were injected with 15 ng of WT or mutant *HERG* cRNA and incubated for 3 days at 19°C.

Electrophysiology. Ionic and gating currents were measured by using the cut-open oocyte vaseline gap recording technique (12) and a CA-1B amplifier (Dagan, Minneapolis). Voltage commands were generated by using PCLAMP8 software (Axon Instruments, Union City, CA), a personal computer, and a Digi-Data 1320 interface (Axon Instruments). Recordings were performed at room temperature (22–24°C). Signals were digitized at 20 kHz and filtered at 5 kHz with an eight-pole Bessel filter.

Microelectrodes were pulled from borosilicate glass capillary tubes to obtain resistances of 0.1–0.5 MΩ when filled with 3 M KCl or CsCl. For ionic recordings, the extracellular solution (top and guard chambers) contained 96 mM NaCl, 4 mM KCl, 2 mM $CaCl_2$, 1 mM $MgCl_2$, and 10 mM Hepes, pH 7.6. The intracellular solution (bottom chamber) contained 120 mM K-glutamate and 10 mM Hepes, pH 7.0. For gating current recordings, the extracellular solution consisted of 120 mM tetraethylammonium (TEA)- Mes, 2 mM Ca-Mes, and 10 mM Hepes, pH 7.4; and the intracellular solution consisted of 120 mM TEA-Mes and 10 mM Hepes, pH 7.4. In a few indicated gating current experiments, 120 mM *N*-methylglucamine (NMG)-Mes was substituted for TEA-Mes. The oocyte was permeabilized by adding 0.1–0.3% saponin to the lower chamber for 2 min. Intracellular K^+ was depleted by clamping the membrane to −10 mV for 30 min. To ensure complete block of HERG channels, the specific HERG blocker MK-499 (50 μM) (13) was added to the external and internal solutions after depletion of intracellular K^+. Qualitatively similar gating currents were recorded in TEA- and NMG-containing solutions, with or without MK-499. The combination of TEA and MK-499 was most effective at eliminating residual ionic current during prolonged step depolarizations. Linear leak and capacitance currents were compensated by analog circuitry

This paper was submitted directly (Track II) to the PNAS office.

Abbreviations: G–V, conductance–voltage; EAG, ether-a-go-go; HERG, human EAG-related gene; HP, holding potential; *Ig*, gating current; Ig_{ON}, on *Ig*; Ig_{OFF}, off *Ig*; Q–V, charge–voltage; TEA, tetraethylammonium.

§To whom correspondence should be addressed. E-mail: michael.sanguinetti@hmbg.utah.edu.

www.pnas.org/cgi/doi/10.1073/pnas.1832721100

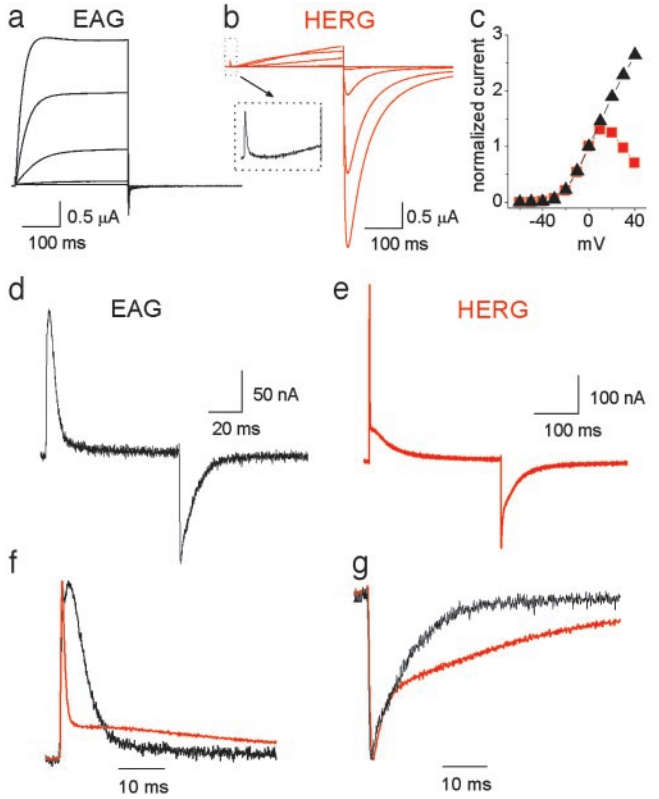

Fig. 1. Comparison of gating and ionic currents for ether-a-go-go (EAG) and HERG K^+ channels. EAG (*a*) and HERG (*b*) ionic current elicited by 300-ms depolarizations ranging from −50 to +30 mV, applied in 20-mV increments from a HP of −110 mV. *Inset* illustrates that a fast gating component of gating current precedes the onset of ionic current activation for the pulse to +30 mV. (*c*) I–V relationship for EAG (black triangles) and HERG (red squares). Current amplitude at the end of a 300-ms depolarization was normalized to the amplitude at 0 mV and the normalized values plotted versus test potential. Shown are EAG (*d*) and HERG (*e*) gating currents elicited by 80-ms (EAG) or 300-ms (HERG) depolarizations to +10 mV from a HP of −110 mV. Normalized and superimposed traces of Ig_{ON} at +10 mV (*f*) and Ig_{OFF} at −110 mV (*g*) for EAG (black) and HERG (red) are compared on the same time scale.

and subtracted on-line by using a p/-8 protocol (14) from a holding potential (HP) of −110 mV. Unsubtracted current records in preliminary experiments indicated the lack of charge movement at potentials negative to −100 mV. In addition, no significant changes in gating currents were observed when the p/-8 protocol was used from a HP of −100 mV or −120 mV. Nonlinear transient currents were not detected in uninjected oocytes, indicating that gating currents detected in HERG-injected oocytes were not contaminated by constitutively expressed channels.

Data Analysis. A measure of intramembrane charge (Q) displacement was obtained by integration of the ON or OFF gating current (Ig) elicited by step changes in membrane voltage. The values of Q versus test potential were plotted and fitted to a Boltzmann function to calculate relative charge, Q_{rel}:

$$Q_{rel} = Q/Q_{max} = 1/[1 + \exp(-zF/RT(V_t - V_{1/2}))], \quad [1]$$

where Q_{max} is the maximum calculated charge moved, V_t is the test potential, $V_{1/2}$ is the half-point of the relationship, z is the effective valence, and F/RT has the usual meaning. The voltage dependence of current activation and inactivation were also calculated by using a Boltzmann function as described (15).

Data were expressed as mean ± SEM. Differences between groups were determined by using the unpaired t test (SIGMASTAT V2.03, SPSS, Chicago). A P value <0.05 was required for statistical significance.

Markov State Model. A Markov state model was constructed by using MODELMAKER3 (Cherwell Scientific, Oxford). Differential rate equations were integrated numerically over 0.01-ms time steps by using Runge–Kutta techniques. Forward rates were calculated as $\alpha = \alpha_0 \cdot \exp(z\alpha \cdot VF/RT)$ and backward rates as $\beta = \beta_0 \cdot \exp(-z\beta \cdot VF/RT)$. Statistical (4, 3, 2, 1) and cooperative (c) factors were used in the independent transitions to reflect the number of subunits available for the transition and the number that have already made the transition (16). For example, for the first subunit transition, before any subunits have moved (S0000), the intrinsic rate for a single subunit is multiplied by four to

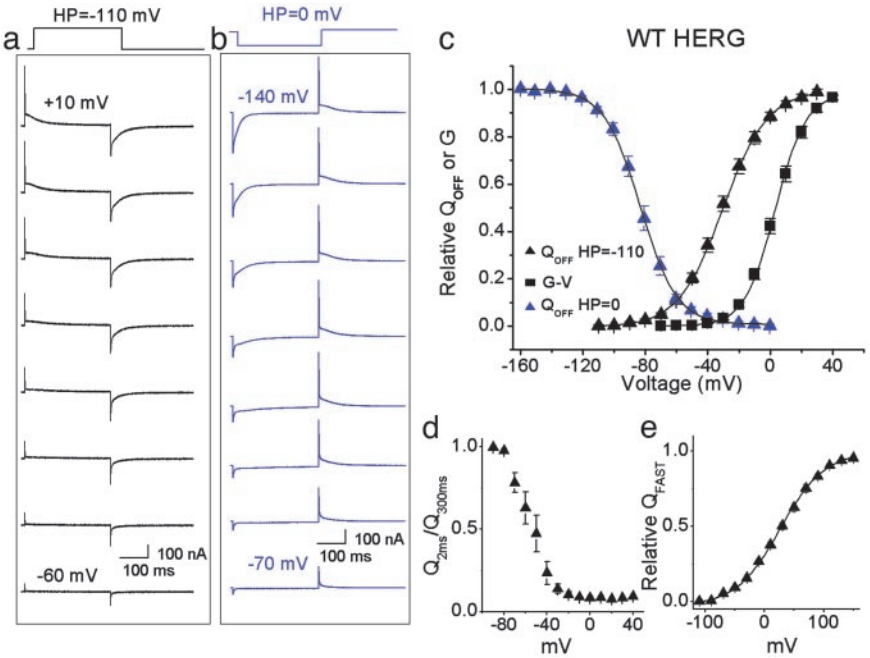

Fig. 2. Properties of WT HERG gating currents. Family of HERG gating currents elicited by 300-ms pulses to the indicated test potential from HPs of −110 mV (*a*) and 0 mV (*b*). Test pulses were applied in 10-mV increments. (*c*) Normalized Q_{OFF}–V and G–V relationships of WT HERG channels. The integral of Ig_{OFF} was normalized for each cell and the mean value plotted versus voltage. The isochronal G–V relationship was determined by tail current analysis of ionic currents elicited with 300-ms pulses. The voltage dependence of Q_{OFF}–V and G–V relationships was determined by fitting data to a Boltzmann function. The $V_{1/2}$ and z were −25 ± 1.2 mV and 1.9 ± 0.06 for the Q_{OFF}–V relationship at a HP of −110 mV (n = 19), −5.6 ± 1.2 mV and 2.4 ± 0.1 for the G–V relationship (n = 9), and −83 ± 2.2 mV and 2.4 ± 0.05 for the Q_{OFF}–V relationship at a HP of 0 mV (n = 7). (*d*) Relative proportion of fast Q_{ON} as a function of test potential. Ig_{ON} was integrated, and the charge moved in the first 2 ms (Q_{2ms}) was expressed as fraction of total charge moved (Q_{300ms}) at each test potential (n = 7). (*e*) Voltage dependence of Q_{FAST}. Fast Ig_{ON} was elicited by 2-ms pulses to potentials ranging from −110 to +150 mV from a HP of −120 mV. Ig_{ON} was integrated after subtracting standing current at the end of the 2-ms pulse, plotted versus voltage and fitted to a Boltzmann function to determine relative Q_{FAST}. The $V_{1/2}$ and z were +28 ± 4.4 mV and 0.7 ± 0.02 (n = 5).

PHYSIOLOGY

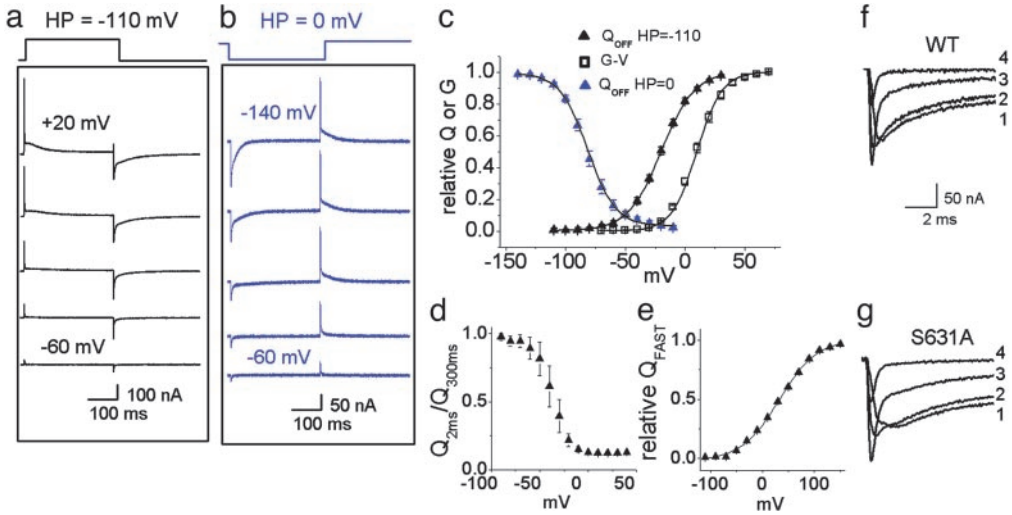

Fig. 3. Gating currents of inactivation-deficient S631A HERG channels. Family of gating currents elicited as in Fig. 2 from a HP of −110 mV (*a*) and 0 mV (*b*). Test pulses were applied in 20-mV increments. (*c*) Normalized Q_{OFF}–V and G–V relationships. The $V_{1/2}$ and *z* were −21 ± 1.4 mV and 1.9 ± 0.1 for the Q_{OFF}–V relationship at a HP of −110 mV ($n = 9$), +9.4 ± 1.4 mV and 2.4 ± 0.1 for the G–V relationship ($n = 7$), and −82 ± 2.2 mV and 2.1 ± 0.1 for the Q_{OFF}–V relationship at a HP of 0 mV ($n = 7$). (*d*) Q_{2ms}/Q_{300ms} as a function of test potential ($n = 4$). (*e*) Voltage dependence of Q_{FAST} was determined as in Fig. 2*e*. The $V_{1/2}$ and *z* were +32 ± 1.5 mV and 0.7 ± 0.01 ($n = 5$). (*f* and *g*) Ig_{OFF} for WT (*f*) and S631A (*g*) HERG elicited by pulses to −110 mV after a 300-ms test pulse to +30 mV (trace 1), 0 mV (trace 2), −30 mV (trace 3), and −60 mV (trace 4).

reflect that four subunits are available to move. Once one subunit has moved (S0001), that factor drops to three and a cooperativity factor *c* is included in both the forward (*c*) and reverse rates (c^{-1}) to reflect the cooperativity that results from having moved one subunit out. No cooperativity results when $c = 1$, negative cooperativity when $c < 1$ and positive cooperativity when $c > 1$. Once three subunits have moved (S0111), the final transition to S1111 has only one subunit left to move, but three that contribute to the cooperativity (c^3 and $c - 3$):

$$\underset{}{\text{S0000}} \underset{1\cdot\beta}{\overset{4\cdot\alpha}{\rightleftharpoons}} \underset{}{\text{S0001}} \underset{2\cdot\beta\cdot c^{-1}}{\overset{3\cdot\alpha\cdot c}{\rightleftharpoons}} \underset{}{\text{S0011}} \underset{3\cdot\beta\cdot c^{-2}}{\overset{2\cdot\alpha\cdot c^2}{\rightleftharpoons}} \underset{}{\text{S0111}} \underset{4\cdot\beta\cdot c^{-3}}{\overset{1\cdot\alpha\cdot c^3}{\rightleftharpoons}} \underset{}{\text{S1111}} \quad [2]$$

Results and Discussion

Comparison of HERG and EAG Gating. Although HERG channels belong to the EAG family, the properties of HERG and EAG ionic current are markedly distinct. EAG channels activate and deactivate rapidly and do not inactivate (Fig. 1*a*). HERG channels activate and deactivate slowly, but inactivate rapidly (Fig. 1*b*). The current–voltage relationship for EAG and HERG channels are compared in Fig. 1*c* and show that inactivation of HERG results in a bell-shaped relationship. To distinguish potential differences in HERG gating associated with activation and inactivation, we compared the gating currents of HERG and EAG. As previously reported for EAG channels (17), gating currents evoked by membrane depolarization (Ig_{ON}) and repolarization (Ig_{OFF}) were rapid in onset and decay (Fig. 1*d*). HERG Ig_{ON} was markedly different from EAG, with a fast transient followed by a very slow decaying component (Fig. 1 *e* and *f*). The fast and slow components of Ig_{ON} differed nearly 100-fold in their decay (τ_{fast}: 0.5 ± 0.02 ms, τ_{slow}: 53 ± 3 ms at +10 mV; $n = 4$). The fast component of Ig_{ON} was discernible in the ionic current records as a small, rapid transient outward current that preceded the onset of ionic current (Fig. 1*b Inset*). The Ig_{OFF} was much slower for HERG than EAG channels (Fig. 1*g*). Thus, HERG gating current is slower than any previously reported voltage-gated ion channel, with a rapid component nearly 100 times faster. We proceeded to characterize the components of HERG gating.

Analysis of HERG Gating Current. Representative HERG gating currents recorded in response to variable test potentials are shown in Fig. 2*a*. The fast component of Ig_{ON} was first detected near −80 mV, well below the apparent threshold for channel opening. The integral of either Ig_{ON} (Q_{ON}) or Ig_{OFF} (Q_{OFF}) provides a measure of the charge moved for a given step in voltage. For most channels $Q_{ON} = Q_{OFF}$. However, similar to EAG channels (17), we found that Q_{OFF} exceeded Q_{ON} at negative membrane potentials where HERG channels open very slowly. At more depolarized potentials, Q_{ON} and Q_{OFF} were nearly equal (e.g., at +10 mV, Q_{ON}/Q_{OFF} was 1.08 ± 0.08, $n = 8$). The $V_{1/2}$ for the Q_{OFF}–V relationship was shifted

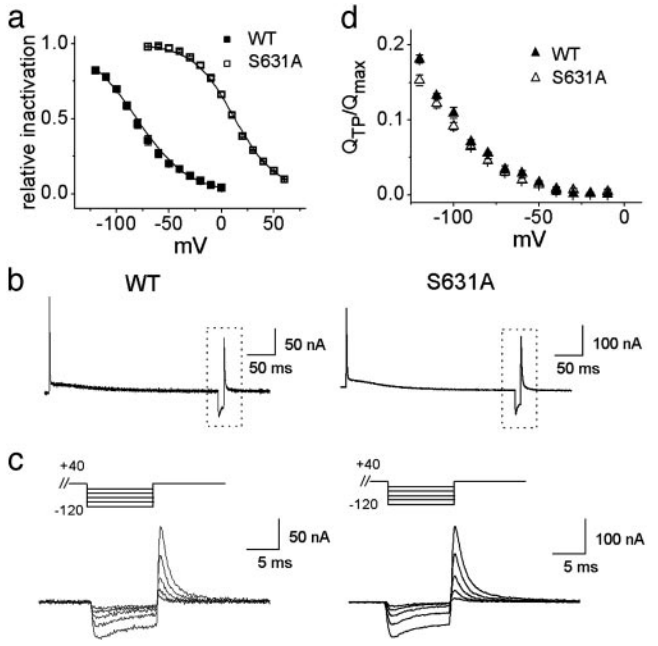

Fig. 4. Comparison of WT and S631A channel inactivation. (*a*) Voltage dependence of ionic current inactivation. Peak current during the test pulse of the triple pulse protocol was plotted as a function of interpulse potential. The $V_{1/2}$ and *z* of the Boltzmann function were −82 ± 2.4 mV and 1.1 ± 0.07 for WT ($n = 3$) and +7.8 ± 5.0 mV and 1.4 ± 0.06 for S631A ($n = 3$). (*b*) Gating currents for WT and S631A HERG elicited by a triple-pulse voltage protocol (prepulse = +40 mV, interpulse = −110 mV, test pulse = +40 mV). (*c*) Expanded time scale of boxed area in *b* for WT (*Left*) and S631A (*Right*) for interpulse potentials ranging from −120 to −40 mV in 20-mV increments. (*d*) Charge measured during test pulse of a triple pulse protocol divided by the maximal Q_{OFF} elicited by a 300-ms-step depolarization (Q_{TP}/Q_{max}) plotted versus interpulse test potential. Because external TEA is known to slow the recovery from and onset of HERG inactivation (3), TEA in the external solution was substituted with 120 mM NMG for experiments shown in *b–d*.

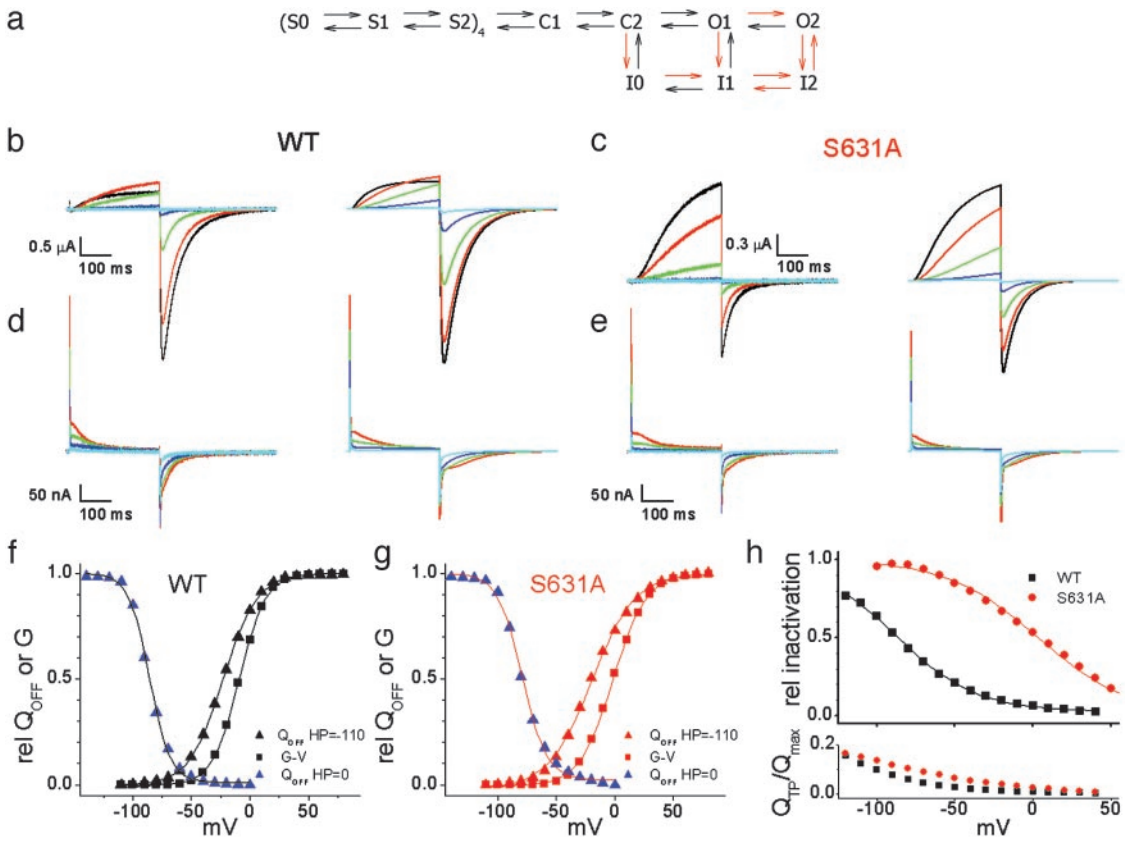

Fig. 5. Markov model of WT and S631A HERG channels. (*a*) Schematic of the Markov state model. The rates and valences for the transitions are presented in Table 1. The forward rates of the transitions marked as red arrows were changed to model S631A behavior as indicated in red text. (*b*) Ionic currents recorded from WT HERG channels (*Left*) and currents predicted by the model (*Right*). Voltages in *b*–*e* are indicated by the following colors: black, +30 mV; red, +10 mV; green, −10 mV; blue, −30 mV; cyan, −50 mV. (*c*) Ionic currents recorded from S631A HERG channels (*Left*) and currents predicted by the model (*Right*). (*d*) Gating currents recorded from WT HERG channels (*Left*) and predicted by the model (*Right*). (*e*) Gating currents recorded from S631A HERG channels (*Left*) and *Ig* predicted by the model (*Right*). (*f*) WT HERG Q_{OFF}–V (HP = −110 mV, $V_{1/2}$ = −23 mV, and z = 1.8; HP = 0 mV, $V_{1/2}$ = −86 mV, and z = 2.9) and G–V curves ($V_{1/2}$ = −9 mV and z = 2.2) predicted by the model. (*g*) S631A Q_{OFF}–V (HP = −110 mV, $V_{1/2}$ = −20 mV, and z = 1.4; HP = 0 mV, $V_{1/2}$ = −79 mV, and z = 2.4) and G–V curves ($V_{1/2}$ = −2 mV and z = 1.8) predicted by the model. (*h*) (*Upper*) Relative inactivation predicted by the model for a triple pulse protocol as in Fig. 4*a*. $V_{1/2}$ and z were −88 mV and 1.0 for WT and +3 mV and 0.9 for S631A. (*Lower*) Q_{TP}/Q_{max} predicted by the model, as calculated in Fig. 4*d*.

−19 mV relative to the isochronal conductance–voltage (G–V) relationship for 300-ms pulses (Fig. 2*c*). The $V_{1/2}$ and z were −25 ± 1.2 mV and 1.9 ± 0.06 for the Q_{OFF}–V relationship (n = 19). The $V_{1/2}$ and z were −5.6 ± 1.2 mV and 2.4 ± 0.1 mV for the G–V relationship (n = 9). Longer pulses (2 s) shifted the $V_{1/2}$ of the G–V relationship to −11 mV as reported (15).

C-type inactivation in Shaker channels is associated with a −50 mV shift in the Q–V relationship when currents are elicited from a HP of 0 mV (18). To determine whether HERG channel gating displays a similar shift, we measured gating currents elicited by stepping between −160 and 0 mV from a HP of 0 mV (Fig. 2*b*). Fast and slow gating components were detected on stepping back to 0 mV after a test pulse to a variable test potential. The total gating charge moved from a HP of 0 mV was similar to that from a HP of −110 mV, but the Q–V relationship was shifted by −60 mV ($V_{1/2}$ = −82.7 ± 2.2 mV, n = 7; Fig. 2*c*). Thus, HERG undergoes a similar negative shift as Shaker in the voltage dependence of Q in response to sustained membrane depolarization.

Is there a unique component of gating current associated with fast inactivation of HERG? Based on kinetics alone, an obvious candidate is the fast component of Ig_{ON}. The relative proportion of fast Q_{ON}, measured from a HP of −110 mV as Q_{2ms}/Q_{300ms}, comprised 0.98 ± 0.01 of the charge moved at −80 mV versus 0.10 ± 0.02 at −20 mV (Fig. 2*d*, n = 7). Thus, the fast gating component constituted the majority of charge moved at potentials below the threshold for channel activation, whereas the bulk of charge displacement at more positive potentials derived from the slow gating component. The voltage dependence of fast Q_{ON} was evaluated by using 2-ms pulses from a HP of −120 mV (Fig. 2*e*). The Q–V relationship for the fast Q_{ON} had a $V_{1/2}$ of +28 ± 4.4 mV and a z of 0.7 ± 0.02 (n = 5), similar to the fast component of fluorescence reported by a probe attached to the S4 domain of HERG (7). Although determined with different pulse protocols, the voltage dependence for fast Q_{ON} was 120 mV more positive than the recovery from inactivation of HERG ionic current (3).

Inactivation-Deficient S631A HERG Gating Currents. To determine whether a component of *Ig* is uniquely related to fast inactivation, we characterized S631A HERG channels by using the same voltage pulse protocols used to study WT HERG. The S631A mutation shifts the voltage dependence of channel inactivation by +100 mV (6). If a major component of charge displacement is associated with inactivation, then differences in the voltage dependence and kinetics for *Ig* of WT and S631A HERG channels should be measurable. In contrast to this prediction, Ig_{ON} and Ig_{OFF} of S631A channels (Fig. 3*a*) and the voltage dependence of the Q_{OFF}–V relationship (Fig. 3*c*) were

similar to WT HERG. When *Ig* was elicited from a HP of 0 mV (Fig. 3*b*), the Q_{OFF}–V relationship for S631A (Fig. 3*c*) was shifted by −61 mV ($V_{1/2} = -82 \pm 2.2$ mV, $n = 5$), compared with a −58 mV shift measured for WT HERG (Fig. 2*c*). The voltage dependencies of the Q_{2ms}/Q_{300ms} relationship and the relative fast Q_{ON} for S631A were also not different from WT (Fig. 3 *d* and *e*).

In Shaker channels, Ig_{OFF} associated with transitions between closed channel states decays rapidly, but once channels transit into the open or inactivated state, the rate of charge return is delayed and slowed (10). A similar pattern was observed for WT HERG channels and despite disparate inactivation properties, the delay and decay of Ig_{OFF} for both S631A and WT channels were similar (Fig. 3 *f* and *g*). For example, after a pulse to +40 mV, the time to peak Ig_{OFF} was 1.6 ± 0.1 ms for WT and 1.9 ± 0.2 ms for S631A. The fast and slow time constants for Ig_{OFF} decay were 4 ± 1 ms and 52 ± 3 ms for WT ($n = 5$) and 4 ± 1 ms and 57 ± 4 ms for S631A ($n = 6$). Thus, Ig_{OFF} for WT and S631A HERG channels are indistinguishable at the resolution of our recordings.

As reported (3, 6), the most striking difference between WT and S631A HERG ionic current is revealed by using a triple-pulse voltage protocol to assess the voltage dependence of channel inactivation. This pulse protocol was used to compare ionic and gating currents of WT and S631A channels. HERG channels were activated and inactivated by a 0.3-s prepulse to +40 mV (WT) or +80 mV (S631A) followed by a 10-ms hyperpolarizing interpulse to a variable potential to rapidly recover inactivated channels into the open state while minimizing deactivation. A third (test) pulse to +40 or +80 mV was applied to assess the relative proportion of channels that recovered from inactivation during the interpulse. The $V_{1/2}$ of ionic current inactivation was shifted +90 mV for S631A compared with WT (Fig. 4*a*). In contrast, gating currents elicited by a triple pulse protocol were indistinguishable (Fig. 4 *b* and *c*). For these recordings, the pre- and test-pulse potentials were +40 mV. The normalized Q–V relationships determined from currents elicited by the test pulse were not different between WT and S631A HERG for interpulse potentials between 0 and −120 mV (Fig. 4*d*), where channel deactivation was minimal. Although we could not detect any obvious differences between the gating currents of WT and S631A, other mutations in HERG that accelerate the rate of deactivation or subtly alter the voltage dependence of activation were associated with concomitant changes in gating currents (Fig. 6, which is published as supporting information on the PNAS web site, www.pnas.org).

A Kinetic Model to Describe HERG Channel Gating. We derived a tetrameric Markov state model for HERG (Fig. 5*a*) based on previous models for Shaker and HERG channels (16, 19, 20). The first two closed transitions were treated independently for each of the four subunits, with positive cooperativity included in the second transition. The remaining closed, open, and inactivating transitions were treated as concerted rearrangements of all four subunits. Based on single-channel recordings, the model incorporates two open states with equal conductances (21, 22). Single-channel data also indicate a high probability of inactivation from a closed state in WT HERG (21, 22). In the model, the C2 → I0 transition becomes dominant compared with C2 → O1 with strong depolarization. Although the fast Ig_{ON} is kinetically similar to fast ionic current inactivation, the model predicts that fast Ig_{ON} is derived primarily from the first independent subunit transition (S0 → S1). By contrast, the gating charge associated with inactivation is delayed and moves either parallel with or subsequent to charge associated with channel opening.

The inactivation-deficient S631A HERG was modeled by slowing the rates of the forward inactivating transitions (C2 → I0, O1 → I1, and O2 → I2), and hastening the rates of the forward O1 → O2 and the reverse I2 → O2 transitions. The rates of the I0 → I1 and I1 → I2 transitions were slowed to preserve microscopic reversibility. The altered transitions are indicated by red arrows in Fig. 5*a*. No changes were made in the charge associated with any of the transitions. Although the model is not a unique solution, it predicts the observed differences in ionic current (Fig. 5 *b* and *c*) and lack of qualitative differences in gating currents (Fig. 5 *d* and *e*) between WT and S631A HERG. The model reproduces the HP-dependent shifts in the Q–V relationships for both channels (Fig. 5 *f* and *g*). The model predicts a 91-mV difference between WT and S631A inactivation half-points (Fig. 5*h* *Upper*), but does not predict identical gating currents associated with recovery from inactivation (Fig. 5*h* *Lower*). Thus, although imperfect, the model can account for the major properties of ionic and gating current of WT and an inactivation-deficient mutant HERG channel.

Table 1. Rates, valences, and cooperatives for the Markov model

Transition	α_0, ms^{-1}	β_0, ms^{-1}	$z\alpha$, e_0	$z\beta$, e_0	c
S0S1	1	1.5	0.2	0.04	1
S1S2	0.15	0.28	0.15	0.05	1.5
S2C1	1	3.49E-4	0.971	1.062	
C2C2	0.024	0.16	0	0	
C2O1	0.03	1.7E-4	1	1.2	
O1O2					
WT	0.2	0.02	0.1	0.8209	
S631A	0.35				
C2I0					
WT	2.5E-2	8.5E-4	1.57	1.84	
S631A	2.5E-4				
O1I1					
WT	0.2	5E-3	0.4	0.8209	
S631A	9E-4				
O2I2					
WT	1	0.05	0.4	0.2	
S631A	0.1	0.15			
I0I1					
WT	0.24	1E-3	0.0109	0	
S631A	0.108				
I1I2					
WT	2.5	0.5	0.3	0	
S631A	0.324	5E-3			

Parameter values for WT and S631A channels were the same unless indicated otherwise.

In summary, we have described gating currents recorded from HERG delayed rectifier K^+ channels. Similar to the findings of Smith and Yellen (7), who monitored fluorescent changes associated with HERG channel gating, we found that gating currents were composed of fast and slow components, suggesting that both techniques reported the same voltage sensor movements. Compared with previously studied voltage-gated K^+ channels, the bulk of HERG gating current is extremely slow and accounts for the slow rate of channel opening. Although a mutation that alters channel inactivation causes substantial changes in ionic currents, it is not associated with a detectable alteration in gating currents.

We thank Riccardo Olcese for invaluable expert advice and Peter Westenskow and Meng San Pun for excellent technical assistance. This work was supported by National Institutes of Health/National Heart, Lung, and Blood Institute Grants HL65299 (to M.C.S.), HL03816 (to M.T.-F.), and HL071391 (to D.R.P.).

1. Keating, M. T. & Sanguinetti, M. C. (2001) *Cell* **104,** 569–580.
2. Nichols, C. G. & Lopatin, A. N. (1997) *Annu. Rev. Physiol.* **59,** 171–191.
3. Smith, P. L., Baukrowitz, T. & Yellen, G. (1996) *Nature* **379,** 833–836.
4. Spector, P. S., Curran, M. E., Zou, A., Keating, M. T. & Sanguinetti, M. C. (1996) *J. Gen. Physiol.* **107,** 611–619.
5. Schonherr, R. & Heinemann, S. H. (1996) *J. Physiol.* **493.3,** 635–642.
6. Zou, A., Xu, Q. P. & Sanguinetti, M. C. (1998) *J. Physiol.* **509,** 129–138.
7. Smith, P. L. & Yellen, G. (2002) *J. Gen. Physiol.* **119,** 275–293.
8. Taglialatela, M., Toro, L. & Stefani, E. (1992) *Biophys. J.* **61,** 78–82.
9. Stefani, E., Toro, L., Perozo, E. & Bezanilla, F. (1994) *Biophys. J.* **66,** 996–1010.
10. Bezanilla, F. (2000) *Physiol. Rev.* **80,** 555–592.
11. Sanguinetti, M. C., Jiang, C., Curran, M. E. & Keating, M. T. (1995) *Cell* **81,** 299–307.
12. Stefani, E. & Bezanilla, F. (1998) *Methods Enzymol.* **293,** 300–318.
13. Lynch, J. J., Jr., Wallace, A. A., Stupienski, R. F., III, Baskin, E. P., Beare, C. M., Appleby, S. D., Salata, J. J., Jurkiewicz, N. K., Sanguinetti, M. C., Stein, R. B., *et al.* (1994) *J. Pharmacol. Exp. Ther.* **269,** 541–554.
14. Armstrong, C. M. & Bezanilla, F. (1977) *J. Gen. Physiol.* **70,** 567–590.
15. Tristani-Firouzi, M., Chen, J. & Sanguinetti, M. C. (2002) *J. Biol. Chem.* **277,** 18994–19000.
16. Zagotta, W. N., Hoshi, T. & Aldrich, R. W. (1994) *J. Gen. Physiol.* **103,** 321–362.
17. Tang, C. Y., Bezanilla, F. & Papazian, D. M. (2000) *J. Gen. Physiol.* **115,** 319–338.
18. Olcese, R., Latorre, R., Toro, L., Bezanilla, F. & Stefani, E. (1997) *J. Gen. Physiol.* **110,** 579–589.
19. Schoppa, N. E. & Sigworth, F. J. (1998) *J. Gen. Physiol.* **111,** 313–342.
20. Lu, Y., Mahaut-Smith, M. P., Varghese, A., Huang, C. L., Kemp, P. R. & Vandenberg, J. I. (2001) *J. Physiol.* **537,** 843–851.
21. Kiehn, J., Lacerda, A. E. & Brown, A. M. (1999) *Am. J. Physiol.* **277,** H199–H210.
22. Zou, A., Curran, M. E., Keating, M. T. & Sanguinetti, M. C. (1997) *Am. J. Physiol.* **272,** H1309–H1314.